Direct Observation of Electron Bernstein Wave heating by OXB-Mode Conversion at low magnetic field in the WEGA Stellarator

Y. Y. Podoba, H. P. Laqua, G. B. Warr, M. Schubert, M. Otte, S. Marsen, and F. Wagner

Max-Planck-Institut fur Plasmaphysik, EURATOM Ass. D-17491 Greifswald, Germany.

E. Holzhauer

Institut fur Plasmaforschung Univ. Stuttgart, D-70569 Stuttgart, Germany.

01.12.2006

The Ordinary-Extraordinary-Bernstein (OXB)-mode conversion process for overdense plasma heating with electron Bernstein waves (EBW) is demonstrated in the WEGA stellarator at low magnetic field (~50mT) at 2.45 GHz. For the first time the conversion from O-wave to X-wave is clearly demonstrated by probe measurements of amplitude and phase of the wave field in the conversion region and supported by two-dimensional full-wave calculations. The propagation and resonant absorption of the Bernstein wave is measured in fast power modulation experiments.

52.35.Hr, 52.50.Sw, 52.55.Hc, 52.70.Gw

Introduction

Magnetized plasmas show magneto-optic properties which can be used for heating and

diagnostics utilizing resonance and cut-off conditions, i.e. Faraday or the Cotton-Mouton effect. As both fusion and technological plasmas generally benefit from operation at high density an important theoretical progress was the development of the XB and OXB mode conversion processes. EBW[1] heating of overdense plasmas by the OXB process has been demonstrated in several fusion devices[2, 3]. In these experiments the frequency is high and the wavelength short compared to the plasma scale lengths. Thus, the WKB approximation is applicable. The mode conversion requires a density gradient with a characteristic normalised density scale length k_0L_n is about 10, where $k_0 = 2p/л_0$ is the wavenumber of the incident wave in vacuum, λ_0 is the free space wavelength, $L_n = \left|n_e/\nabla n_e\right|_{UHR}$ is the characteristic density scale length at the upper hybrid resonance (UHR) layer and n_e is the plasma electron density. Direct XB-conversion heating is used in experiments with a relatively low magnetic field, as in CDX-U[4] and TST-2[5]. There, the required normalised gradient length ($k_0L_n \sim 0.3$) was achieved by density profile steepening with local limiters in front of the antenna[6]. In our new approach for low frequency OXB heating the density profile must be flattened to achieve k_0L_n of 1-20. In addition, the WKB-approximation fails and the mode conversion process requires a full wave treatment. In this paper we describe the successful application of the OXB heating scheme to the low-field stellarator WEGA[7]. The mode conversion region is placed into the scrape-off plasma outside the separatrix, where the density scale length is typically 10 cm, which results in a k_0L_n value of 5 for the 2.45 GHz vacuum wavelength (λ=12.24cm). In addition to the technological aspects, the application of OXB at long wavelengths provides a unique opportunity to investigate the mode conversion process and the Bernstein wave absorption in more detail using radially resolved measurements of the phase and amplitude of the waves involved. The EBW absorption process is investigated by temporal modulation of the microwave source and observation of the concomitant oscillations

in electron temperature and density. A two-dimensional Finite-Difference Time-Domain (FDTD) full wave code was developed to compare calculated and measured microwave propagation and mode conversion results.

Theory and simulations

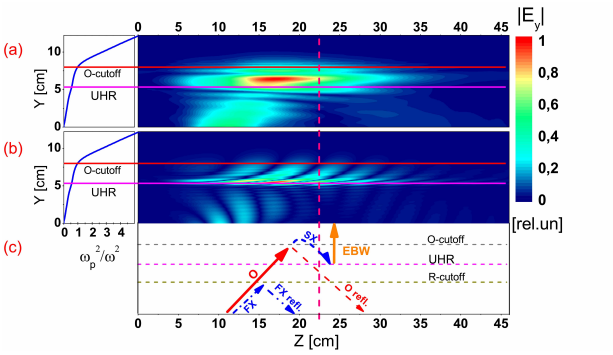

Fig.1. (colour online) Full-wave calculation of the OX conversion process. Time averaged (a) and instantaneous (b) y-component of the wave E field distribution. The normalised density profile is shown on the left side of each plot. The vertical dashed line indicates the position where the experimental results are obtained. The arrows illustrate the waves propagation in mode conversion processes (c).

In the OXB mode conversion process[8] first an externally launched O-mode is coupled to a slow X-mode (SX) in the region of the O-mode cutoff layer ($n_e=n_{e\_cutoff}=7.5\times10^{16}\,m^{-3}$). The SX-mode propagates back to the UHR layer where it is converted into an electrostatic EBW (B-mode see Fig.1c). The EBW propagates into the overdense plasma and is absorbed in the cyclotron resonance region[9]. This method requires launching the radio frequency (RF) power with O-mode polarisation and an optimal oblique orientation to the external magnetic field. The efficiency of

the O-SX transition process in the two dimensions is given by Mjølhus[10], $\tau_{O-SX} = \exp\left[-\pi k_0 L_n \sqrt{2Y}(1+Y)(N_{z\_opt} - N_z)^2\right]$ where $\vec{N} = \vec{k}c/\omega$, and $Y = \omega_c/\omega$ is the ratio between the electron cyclotron frequency and the wave frequency. The maximum of τ_{O-SX} is at the optimal angle $и_{opt} = \arccos\left(\sqrt{Y/(Y+1)}\right)$ between the incident wave vector $\vec{k}$ and the external magnetic field, where $и_{opt}$ = 50° for our experimental conditions. Even though, the equation for $и_{opt}$ is obtained in the WKB approximation limit, which is not satisfied in WEGA at 2.45 GHz, the OXB conversion process is not fully described by the WKB approximation but requires a full-wave calculations[11]. We have developed a FDTD code to perform and compare these calculations with experimental results. The code calculates the full-wave solution of the OXB conversion process using a cold plasma slab model, as this provides a good approximation to the wave behaviour in the OX-conversion and UHR regions. The code solves Maxwell's equations on a two dimensional grid in a horizontal plane near the heating power source in the cold fluid plasma model. The solution region is bounded with numerical absorbers.

Fig.1 shows the calculated time averaged E_y (1a) and instantaneous E_y amplitude (1b). Here y and z are the radial and toroidal coordinates in the equatorial plane. The insert to Fig.2c shows the position of the calculation slab at the antenna. The code uses the measured plasma density and the vacuum magnetic field distribution as input data. The heating power source is simulated using the vacuum antenna field pattern as shown in Fig. 2c.

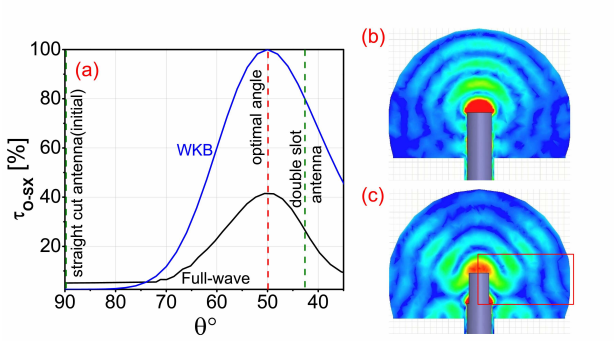

Fig.2. (colour online) Left: (a) Comparison of the O to SX mode conversion efficiency τ_{O-SX} for the WKB and full-wave approximation. Right: HFSS calculations of the antenna patterns in vacuum for the open waveguide (b) and double slot (c) antennas. Red rectangle on the plot (c) corresponds to the full-wave calculation region shown in Fig.1.

The O-mode radiation emanating from the microwave source located at the bottom left of Fig.1a and b propagates towards the O-cutoff layer where it is converted into the SX–mode. The unconverted part of the radiation is reflected. The SX mode is resonant near the UHR layer where, due to its short wavelength, it is absorbed which is modelled with a numerical viscosity term. The artificial damping allows the estimation of the O-SX conversion efficiency by comparing the transmitted heating power with the unconverted power returned to the absorbing boundary. In a real finite temperature plasma the SX-wave is converted into a Bernstein wave at the UHR layer.

Fig.2a shows the result of the computations of the O-SX conversion efficiency as a function of the launch angle θ. The WKB calculation uses $\Delta k_{\parallel} c/\omega=0$, while in the full-wave calculations a Gaussian beam with full width half maximum $\Delta k_{\parallel} c/\omega=0.58$ (or $\Delta\theta \approx 40°$) is used. A broad maximum of O-SX conversion efficiency (~40%) is found near $\theta=50°$, which is the same as that

found in the WKB approximation. The relatively low calculated mode conversion efficiency is due to the wide $\vec{k}$ spectrum of the incident RF beam. In addition, the original antenna polarisation mixture of O-mode (65%) and X-mode (35%) is used. This leads to the reflection of the X-mode component at the R cutoff layer shown by dash dot arrows (FX) near the high frequency (HF) source in Fig.1c. The polarisation dependence was also investigated in the full-wave calculations. For a narrower $\vec{k}$ spectrum and optimised elliptical polarisation of the launched wave, the maximum calculated efficiency reaches ~70%. The minimal reasonable for FDTD value of $\Delta k_{\parallel} c/\omega$~0.2 was used in this calculation.

Experiment and results

WEGA is a medium-sized classical l=2, m=5 stellarator, with major radius R≈72 cm and maximum minor plasma radius a≈11.5 cm. The plasma is generated by up to 26 kW of 2.45GHz ECRH power in a steady state discharge typically for 30 s in Hydrogen, Helium and Argon.

The 83 mm Ø waveguide with two slots in the side wall (10 cm length and 64° angular width) showed the best heating performance. Only the TE11 mode can propagate in this waveguide at 2.45GHz. Thus, producing HF emission linearly polarised in the horizontal plane. The ECRH power is launched into two lobes with corresponding $\theta = \pm 42°$ as shown in Fig.2c. This is the closest to the ideal θ=50° that could be achieved within the space limitations. The antenna patterns are calculated for vacuum conditions since the emission is at a distance of ~10 cm outside the LCFS, where $n_e < n_{e\_cutoff,}$ and the pattern are not significantly perturbed by the plasma. Table 1 shows the improvement of the numerically calculated OX conversion efficiency τ_{O-SX} and improved plasma performance using the double-slot antenna in comparison to that of an open waveguide of the same diameter (the Fig.2b).

	Open waveguide	Double slot
τ_{O-SX} 9	6.7 %	20%
τ_{O-SX} full wave	5.2 %	25%
$n/n_{e\ cutoff}$	1.5 (hollow profile)	12 (peaked profile)
T_e (eV)	<6	<20

Table 1. Calculated O to SX mode conversion efficiency for WKB and full-wave approximations along with measured electron densities (n_e normalised to the cutoff density) and temperatures (T_e) for the open waveguide and the optimised double slot antennas. The efficiency calculations use the antenna patterns computed with the HFSS code shown in Fig.2b,c.

The mode conversion itself could be investigated by direct spatially resolved measurements of the amplitudes and phases of the wave fields in the mode conversion region. When an O-mode is converted into an X-wave, the waves radial E-field amplitude rises close to the UHR layer and its phase jumps along the radial coordinate R. We measured the electric field of the waves with a small electrostatic probe[12] and their magnetic field with two magnetic loop probes oriented perpendicular and parallel to the toroidal magnetic field. The electrostatic probe is designed to be sensitive to short wavelength of longitudinal waves, expected in the SX-mode near the UHR layer[13]. The phase of the E-field is measured with a heterodyne system that mixes the RF wave frequency down from 2.45 GHz to 128 MHz. The n_e profile and thus the position of the UHR is simultaneously measured with a set of Langmuir probes near the heating antenna at the position of the HF probe.

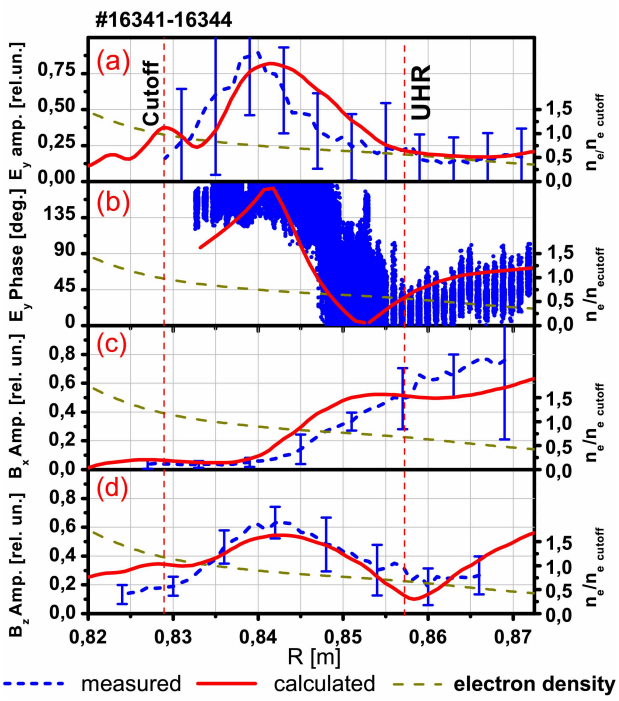

Fig.3. (colour online) Radial profiles of measured and full-wave calculations of E_y amplitude (a), E_y phase (b), B_x (c) and B_z (d) wave components. Calculated (full wave) and measured values are compared. Also the density profile is shown and the locations of the cutoff and the UH-resonance are given.

Fig.3a and b show the good agreement between the measured and calculated (FDTD) phases and amplitudes of the E_y-component (X-wave). The E_y amplitude peaking and phase jump of ~180° near the UHR confirm the existence of the UHR layer in the WEGA plasma and could be reproduced by the FDTD calculations. Fig.3c and d show the HF magnetic field components (B_x and B_z) of the wave measured by the loop probes in comparison with the FDTD results. B_x and B_z correspond to the O-mode and the X-mode respectively. The results of the HF B-field measurements also agree well with the full-wave calculations. B_x decreases near the cutoff layer

and B_z increases between the cutoff and UHR layers indicating the O to SX-mode conversion near the cutoff region. B_z also increases between the UHR layer and the chamber wall (Fig.4d) indicating the presence of parasitic X-mode component in the source emission.

The presence of the Bernstein wave – the final step of the conversion– is shown in heating power modulation experiments. The power is modulated at 12 kHz on a timescale faster than the typical ~1 ms confinement time in WEGA. The perturbation amplitude represents the power deposition while the slope in the phase shows the direction of energy propagation away from the power deposition region. Both are measured with Langmuir probes, which are positioned in the equatorial plane of the WEGA 144° from the heating antenna position in toroidal direction; thus should not be perturbed by the HF-field.

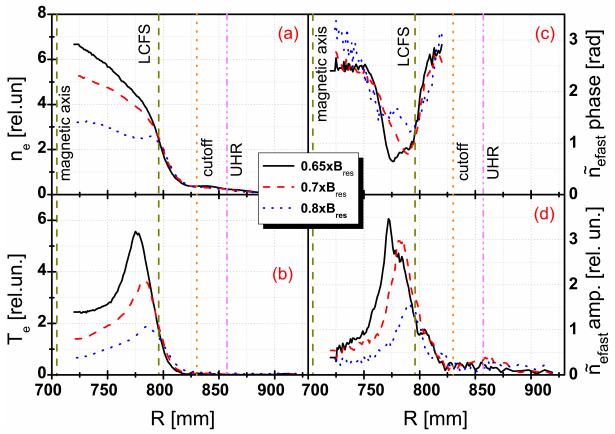

Fig.4. (colour online) Plasma parameters measured by Langmuir probes during power modulation experiments: (a) relative electron density profile, (b) relative thermal electron temperature profile, (c) relative phase and (d) amplitude of the perturbation of the fast electron population for a range of magnetic fields, where B_{res}=87 mT corresponds to the electron cyclotron resonant field at 2.45 GHz. The positions of the last closed flux surface (LCFS), the O-mode cutoff layer and UHR layer are indicated with vertical lines. Heating

power is 3kW.

The density, thermal electron temperature and fraction of fast electrons are determined from Langmuir probe measurements using a two-temperature model[14]. A set of four probes is used at fixed biases of -90V, -25V, 0V and 20V. The probes are separated from each other by 5 mm in poloidal direction and are radially scanned across the plasma. Even though the probe characteristic is estimated by 4 points only and thus the absolute accuracy of the plasma parameters is less than those from the full-characteristic-swept single probe, the relative T_e and n_e profiles are reproduced quite well. The absolute values of typically $T_e \sim 12$ eV and $n_e \sim 10^{18}$ m^{-3} were measured by a slowly sweeping single pin probe and a central line of sight microwave interferometer. Absolute calibration is not necessary for modulation experiments. The density and the fast electron fraction are proportional to the ion saturation current at the -90V biased probe and to the difference of currents at -90V and -25V biasing respectively. Fig.4 shows results of the plasma perturbation measurements for a range of magnetic fields. The fast electron density perturbation (Fig.4d) is largest and strongly localised inside the last closed flux surface (LCFS) in the overdense plasma region. This indicates the power deposition location. No significant perturbation is found near the UHR layer; no notable power deposition is observed in this region. The phase (Fig.4c) shows the propagation of the perturbation away from the deposition region, which is explained by hot electron transport.

Fig.5a shows that the thermal electron temperature is perturbed in the same manner as the fast electrons but with a larger phase shift in the deposition region, indicating the thermalisation of the fast electrons.

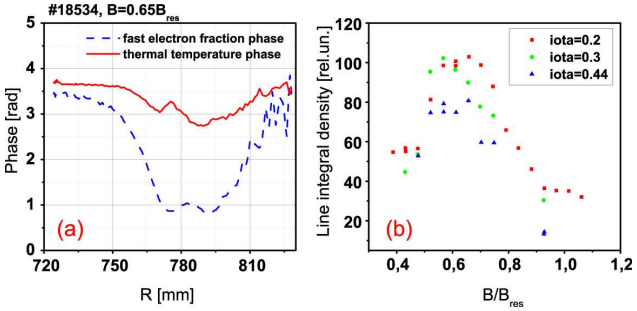

Fig.5. (colour online) (a) Phases of the perturbation of the fast electron fraction and of the thermal electron temperature measured in the optimal magnetic field configuration (same discharge conditions as the solid curve in Fig.4) (b) Line integrated density measured in toroidal magnetic field scan experiments for a range of rotational transforms iota.

The magnetic field dependence of the power deposition location (Fig.4d) provides clear evidence of local resonant EBW heating of the overdense plasma. The absorption is concluded to be strongly Doppler-shifted[8] to lower frequencies peaking at $B=0.65\times B_{res}$, where the maximum achieved line integrated density is also observed, as shown in Fig.5b. This indicates a resonant interaction of the EBW, with a large refractive index component directed along the vacuum magnetic field, with high parallel velocity suprathermal electrons.

Conclusion

Highly over-dense plasma production has been achieved using OXB heating in the WEGA stellarator at low magnetic field. The conversion from O-wave to X-wave was demonstrated by direct measurements of the wave field in the conversion region. The results were supported by full wave calculations. The propagation and resonant absorption of Bernstein waves was measured in fast power modulation experiments. It was shown that the Bernstein waves are

absorbed by supra-thermal electrons with a strongly Doppler shifted cyclotron resonance. Full wave simulations show that a much higher OXB conversion efficiency can be obtained if the heating antenna is designed to emit the HF wave with optimal elliptical polarisation and a narrow $k_{\parallel}$ spectrum. The experiments demonstrate that OXB-mode conversion heating is not restricted to high magnetic field fusion devices but is also applicable in low magnetic field plasma experiments for basic plasma physics research and industrial applications.

---

[1] Ira I. Bernstein, Phys. Rev. **109**, 10 (1958).

[2] A. Mück, et. al. , 32nd EPS Conference on Plasma Phys., Tarragona, ECA Vol.29C, P-4.110. (2005).

[3] H. P. Laqua, V. Erckmann, H.J.Hartfuss, H. Laqua, Phys. Rev. Lett. **78**, 3467 (1997).

[4] P. C. Efthimion, et. al., 19th IAEA Fusion Energy Conference, Lyon, France, P2-12, (2002).

[5] S. Shiraiwa, et. al., Phys. Rev. Lett. **96**, 185003-1 (2006).

[6] G. Taylor, et. al., Physics of Plasmas **10,** 1395 (2003).

[7] M. Otte, et. al., 30th EPS Conference on Plasma Phys., St.Petersburg, ECA **27A**, P-1.9 (2003).

[8] J. Preinhaelter and V. Kopeck´y, Plasma Phys. **10**, 1 (1973).

[9] M. Bornatici, Plasma Phys. Control. Fusion **28 No 4**, 629-645 (1986).

[10] E. Mjølhus, Plasma Phys. **31**, 7 (1984).

[11] S. Nakajima and H. Abe, Phys. Lett. A **124 #4,5**, 295 (1987).

[12] F. Leuterer, Plasma Phys. **14**, 499-521 (1972).

[13] F. Chen, Introduction to Plasma Physics and Controlled Fusion (Plenum Press, 1984),

Vol. **1**, p.123-126.

[14] P. C. Stangeby, Plasma Phys. Control. Fusion **37**, 1031-1037 (1995).